Flexoelectricity in soft elastomers and the molecular mechanisms underpinning the design and emergence of giant flexoelectricity

Matthew Grasinger[a,b,1], Kosar Mozaffari[c,1], and Pradeep Sharma[c,d,2]

[a]Materials and Manufacturing Directorate, Air Force Research Laboratory, WPAFB, OH 45433, USA; [b]UES Inc., Dayton, OH 45432, USA; [c]Department of Mechanical Engineering, University of Houston, Houston, TX 77204, USA; [d]Department of Physics, University of Houston, Houston, TX 77204, USA

Soft robotics requires materials that are capable of large deformation and amenable to actuation with external stimuli such as electric fields. Energy harvesting, biomedical devices, flexible electronics and sensors are some other applications enabled by electro-active soft materials. The phenomenon of flexoelectricity is an enticing alternative that refers to the development of electric polarization in dielectrics when subjected to strain gradients. In particular, flexoelectricity offers a direct linear coupling between a highly desirable deformation mode (flexure) and electric stimulus. Unfortunately, barring some exceptions, the flexoelectric effect is quite weak and rather substantial bending curvatures are required for an appreciable electro-mechanical response. Most experiments in the literature appear to confirm modest flexoelectricity in polymers although perplexingly, a singular work has measured a "giant" effect in elastomers under some specific conditions. Due to the lack of an understanding of the microscopic underpinnings of flexoelectricity in elastomers and a commensurate theory, it is not currently possible to either explain the contradictory experimental results on elastomers or pursue avenues for possible design of large flexoelectricity. In this work, we present a statistical-mechanics theory for the emergent flexoelectricity of elastomers consisting of polar monomers. The theory is shown to be valid in broad generality and leads to key insights regarding both giant flexoelectricity and material design. In particular, the theory shows that, in standard elastomer networks, combining stretching and bending is a mechanism for obtaining giant flexoelectricity, which also explains the aforementioned, surprising experimental discovery.

Flexoelectricity | Elastomers |

Fig. 1. Schematic of a soft robotic appendage, deforming in order to grab an object due to electrical stimuli.

harvesting (12–14), stretchable electronics (15–18), and of course robotics (12, 19, 20). As a compelling illustration of applications, we refer the reader to fascinating recent works on using magnetic actuation to achieve a soft robot made essentially of a rubber filament that is capable of being steered

1. Introduction

Typical *hard* materials such as ceramics have elastic moduli in the order of several hundreds of giga-Pascals. Their deformation, under appropriate levels of mechanical forces, is barely discernible to the naked eye. On the other end of the spectrum, a change of area of nearly 1700% has been demonstrated for an acrylic membrane (1). While both *hard* and *soft* materials have their respective usage, there are important technological imperatives to consider highly deformable soft materials. An oft-quoted example is that of a robotic appendage clasping and moving an object (Fig 1). This requires the capability of large deformation. Ideally, we also hope that such a motion is accomplished through the application of a stimulus that is easily applied (e.g. an electrical field through a battery) and with a modest expenditure of energy. Soft materials that are highly deformable, tough (2), and respond easily to stimuli such as electric field (the focus of this work) have wide applications: biomedical prostheses and devices (3–7), shape-conforming sensors (8–11), energy
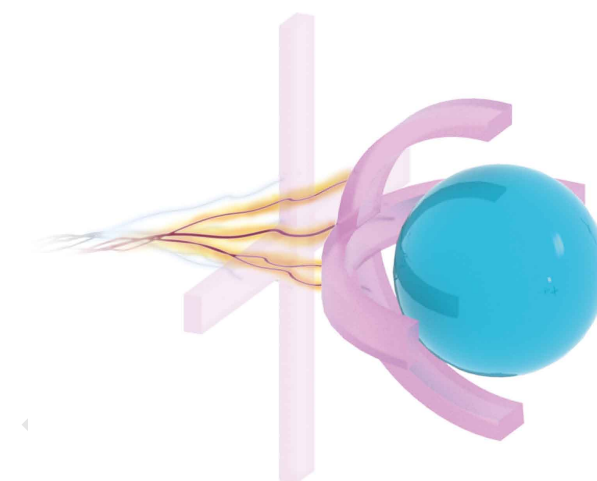
Significance Statement

The molecular-scale phenomena that lead to the emergence of the flexoelectric effect in elastomers are not well understood. We present a molecular-to-continuum scale theory and show it to be valid for common types of elastomers. We unravel a mechanism for achieving giant flexoelectricity–which finds support in prior experimental results. The multiscale theory is then leveraged for material design and we propose specific modalities for (1) the emergence of piezoelectricity, (2) tuning the direction of flexoelectricity, and (3) flexoelectricity which is invariant with respect to spurious deformations. These developments may pave the way for the future development of efficient soft energy harvesters, sensors and actuators, and may prove useful for high degree of freedom soft robots and artificial muscles.

[1]Authors M. G. and K.M. contributed equally to this work.

[2]To whom correspondence should be addressed. E-mail: psharma@uh.edu

through the complex cerebrovascular system with aneurysms (20).

The electromechanical coupling that we *hope* for a soft material to possess is *piezoelectricity*. Materials that are piezoelectric permit a direct and a linear relation between the development of an electric field when subjected to a mechanical stress, and vice-versa. Piezoelectricity can be shown by a linearized relation between polarization($\mathbf{P}$) and the strain tensor($\boldsymbol{\varepsilon}$) as $P_i \sim \mathcal{D}_{ijk}\varepsilon_{jk}$ where $\boldsymbol{\mathcal{D}}$ is a third order tensor reflecting the piezoelectric properties of the material. Unfortunately, piezoelectricity requires the atomic structure of the material to conform to a rather stringent set of symmetry conditions found only in certain hard ceramics. The rather few piezoelectric polymers such as PVDF are (relatively speaking) fairly stiff[*]. Therefore, the electromechanical coupling mechanism that we rely on in the context of soft dielectric elastomer is the Maxwell stress effect or electrostriction—indeed these are the precise mechanisms operative in the example we quoted in the preceding paragraph involving the nearly 1700% areal increase in the acrylic membrane (1). Both the Maxwell stress effect and electrostriction are universally present in all dielectrics where the induced mechanical strain $\boldsymbol{\varepsilon}$ scales with the square of the applied electric field E^2. There is no converse effect hence applications such as energy harvesting and sensing are not easily possible. Further, rather high electric fields must be imposed to generate sufficient forces for an appreciable actuation. An exciting alternative is to embed frozen charges and dipoles in soft matter to create so-called electrets (21–26). Through the interaction of pre-existing immobile charges, electrostriction, and the inherent softness of the material, electrets effectively act as piezoelectrics[†]. While this is a promising research avenue, a key impediment in the use and development of electret materials is that the frozen external charges are only meta-stable and have a propensity to leak out–especially at elevated temperatures and under humid conditions (30).

Having established the relevant context regarding electromechanical coupling mechanisms in soft materials, we now turn to a yet another phenomenon–*flexoelectricity*–which has generated much recent attention (31–33). Briefly, it is the coupling between polarization and strain gradients and can be illustrated by $P_i \sim f_{ijkl}\left(\partial\varepsilon_{jk}/\partial x_l\right)$ where $\boldsymbol{f}$ is a fourth order tensor embodying the flexoelectric behavior of the material. Like electrostriction, flexoelectricity is also a universal phenomenon which occurs in all insulating materials. In non-piezoelectrics, the symmetry of the charge density throughout the material is such that the dipole moment per unit volume, i.e. polarization, vanishes. A homogeneous deformation cannot break the symmetry of the ground state charge density; however, strain gradients can and do, thereby inducing polarization. Very interestingly, the flexoelectric effect has been used to create apparently piezoelectric materials without using piezoelectric materials (33–36) and has broad-ranging applications in energy harvesting (37–43),

and sensors and actuators (44–47). The phenomenon also appears to be implicated in several biophysical functions, e.g. the mammalian hearing mechanism (48–50). A notable aspect of flexoelectricity is the associated size-effect (31). The developed polarization due to flexoelectricity scales with the gradient of the strain. Large strain gradients are most easily produced when feature size is small (e.g. beam thickness, size of embedded inclusions in a composite) and indeed, at least for hard materials, the phenomenon becomes appreciable only at the nanoscale. For soft matter, due to the corresponding lower elastic modulus, a non-trivial flexoelectric response is even possible at micron-length scales (42, 51, 52). As a notable example, Deng et. al. (51) exploited flexoelectricity to design soft materials whose apparent piezoelectric strength is nearly 20 times larger than the hard ferroelectrics like barium titanate with feature sizes of the order of 0.6 microns.

The phenomenological theory of flexoelectricity with various degrees of sophistication and nuances, appears to be now well-developed (e.g. (32, 53, 54)). In the context of soft matter, a first attempt appeared in (51) and we highlight a more recent paper by (54) that is specifically targeted towards proper accounting for large deformations and the correct interpretation of the flexoelectric matter property tensor for large deformations. Significant efforts have also been expended towards computational approaches (e.g. (54–57)). At the other end of the scale-spectrum, extensive research has also ensued on the microscopic underpinnings of the phenomenon. The atomistic-scale mechanisms for flexoelectricity are now relatively well understood for crystalline materials (58–62), liquid crystals (63, 64), and 2D materials (65–70). However, a similar molecular-scale understanding of the flexoelectricity of elastomers has remained elusive (31). This is a key impediment in the design of next-generation soft materials that exhibit substantive flexoelectricity. The flexoelectric coefficients of most soft polymers (like elastomers) exhibit rather modest values. Attempts were made in (71) and (72) to explain flexoelectricity in elastomers through quasi-1D microscopically-based models which utilized linear elastic chains connecting neutral, positive, and negative ions and a kind of free volume theory, respectively. These models are useful to assess the order of magnitude of the flexoelectric effect in elastomers but can hardly capture the nuances of the actual mechanisms and thus are of limited utility for designing materials. The state of affairs is complicated further by experiments which indicate a wide range of flexoelectricity in polymers (73, 74). In this work, we take inspiration from the fact that statistical mechanics and polymer network modeling have explained much of what we understand about the microscopic underpinnings of elasticity (75–78) in elastomers. More recently, a similar success has also been achieved in the context of electroelasticity (79–81) which has inspired our current approach.

In this work:

1. We create a molecular-scale theory for the emergent flexoelectricity of elastomers with polar monomers. The molecular-scale theory is quite general; it is valid for two of the most common theoretical models for polymers: the freely jointed chain and the wormlike chain.

---

[*] Their elastic modulus is of the order of a few GPa's while the soft materials that are highly deformable often need to have stiffness in the KPa range

[†] Detailed theoretical framework outlining the conditions for when electrets act a piezoelectric or even pyroelectric are available here (26, 27). Other illustrative examples may be found in the literature (25, 28, 29).

2. We provide an explanation for the rather wide and non-intuitive range of flexoelectric properties measured for polymers and specifically explain the unusually large values obtained when stretching and bending are combined.

3. We provide an interpretation of understanding microscopic flexoelectricity using the notion quadrupolar moments and leverage this connection to develop material design principles for tuning the direction of the flexoelectric effect, as well as for stretch-invariant flexoelectricity.

4. Finally, we provide simple and clear guidelines to design soft elastomers with giant flexoelectricity.

2. Statistical mechanics of the electroelasticity of a freely jointed chain

As a starting point, we derive the free energy of a polymer chain in a fixed ambient temperature, T, with at a fixed end-to-end vector, $\boldsymbol{r}$, subjected to a constant electric field, $\boldsymbol{E}$. We work in the constant electric field ensemble as a matter of convenience and will eventually use a Legendre transformation to arrive at the Helmholtz free energy. To work in this ensemble, we need the variation of the electric field due to the presence of monomer dipoles to be negligible; that is, the monomers need to be approximately non-interacting[‡]. Such an assumption is quite reasonable c.f. (82) and §1 of the SI where we use Markov chain Monte Carlo calculations to prove this point.

We assume that the energy required to deform an individual monomer is much greater than kT; and, hence, we model the monomers as rigid with length b. For the freely jointed chain, monomers are also free to rotate about their neighboring bonds. We denote the number of monomers per chain as n, the chain stretch as $\gamma := r/nb$, and the orientation of a monomer as $\hat{\boldsymbol{n}}$ so that $\boldsymbol{r} = b\sum_{i=1}^{n} \hat{\boldsymbol{n}}_i$. By assumption, the monomers are polar; or, in other words, have a permanent dipole attached to them. In general, the dipole vector, $\boldsymbol{\mu}$, need not be aligned with $\hat{\boldsymbol{n}}$. However, we do assume that the dipole is a linear transformation of $\hat{\boldsymbol{n}}$; i.e. $\boldsymbol{\mu} = \boldsymbol{M}\hat{\boldsymbol{n}}$. If, for example, a dipole of fixed magnitude is attached rigidly to the monomer such that it rotates with the monomer, then $\boldsymbol{M} = \mu\boldsymbol{Q}$ where $\boldsymbol{Q} \in \mathrm{SO}(3)$. In any case, the electric potential of a monomer depends on its orientation. Let $\boldsymbol{\mathcal{E}} := \boldsymbol{M}^T\boldsymbol{E}$. Then the electric potential of a monomer is given by the expression:

$$u = -\boldsymbol{\mu} \cdot \boldsymbol{E} = -(\boldsymbol{M}\hat{\boldsymbol{n}}) \cdot \boldsymbol{E} = -\boldsymbol{\mathcal{E}} \cdot \hat{\boldsymbol{n}}. \qquad [1]$$

In order to formulate the partition function, we divide the unit sphere into $\mathcal{N}$ infinitesimal patches of area with unit normal $\hat{\boldsymbol{n}}_i, i = 1, 2, ..., \mathcal{N}$. Let m_i denote the number of monomers in the chain with direction $\hat{\boldsymbol{n}}_i$. Then,

$$\mathcal{Z} = \sum_{\{m_j\}}' \left\{ \exp\left[\beta \sum_{i=1}^{\mathcal{N}} m_i \boldsymbol{\mathcal{E}} \cdot \hat{\boldsymbol{n}}_i\right] \frac{n!}{\prod_{i=1}^{\mathcal{N}} m_i!} \right\}, \qquad [2]$$

where $\beta = 1/kT$ and the prime over $\{m_j\}$ denotes that the summation is over all of the collections of population numbers that satisfy the constraints: $\sum_i m_i = n$ and $b\sum_i m_i\hat{\boldsymbol{n}}_i = \boldsymbol{r}$.

Enumerating over all of the terms in Eq. (2) is difficult in general. Instead, we approximate the logarithm of the sum by the logarithm of its maximum-term and, taking $\mathcal{N} \to \infty$ (i.e. the continuum limit of the population numbers), arrive at a mean-field theory. In doing so, we find that

$$\rho(\hat{\boldsymbol{n}}) = C \exp[\beta\boldsymbol{\mathcal{E}} \cdot \hat{\boldsymbol{n}} + \boldsymbol{\tau} \cdot \hat{\boldsymbol{n}}], \qquad [3]$$

where ρ is a probability density function associated with finding a monomer with some direction $\hat{\boldsymbol{n}}$, and C and τ are Lagrange multipliers that are determined by enforcing the continuum analog of the normalization and end-to-end vector constraints, respectively:

$$n = \int_{\mathbb{S}^2} \mathrm{d}A\, \rho, \quad \frac{\boldsymbol{r}}{b} = \int_{\mathbb{S}^2} \mathrm{d}A\, \rho\hat{\boldsymbol{n}}. \qquad [4]$$

Once the unknown multipliers have been determined, the closed-dielectric free energy, $\mathcal{F}$, is approximately

$$\mathcal{F} = -\frac{1}{\beta}\ln\mathcal{Z} \approx \int_{\mathbb{S}^2} \mathrm{d}A\, \rho u + \frac{1}{\beta}\int_{\mathbb{S}^2} \mathrm{d}A\, \rho\ln\rho. \qquad [5]$$

Let $\boldsymbol{\xi} := \beta\boldsymbol{\mathcal{E}} + \boldsymbol{\tau}$. Then the solution for C and $\boldsymbol{\xi}$ is well-known (83) and

$$C = \frac{n\xi\operatorname{csch}\xi}{4\pi}, \quad \boldsymbol{\xi} = \mathcal{L}^{-1}(\gamma)\hat{\boldsymbol{r}}, \qquad [6]$$

where $\xi = |\boldsymbol{\xi}|$, $\hat{\boldsymbol{r}} = \boldsymbol{r}/r$, and $\mathcal{L}^{-1}$ is the inverse Langevin function. Based on cursory examination of Eq. (6), it may seem somewhat surprising that ρ is independent of the electric field and is, in fact, equivalent to the ρ that maximizes the entropy. However, it is easy to show that this is indeed the ρ which minimizes the free energy for any monomer potential energy which is linear in $\hat{\boldsymbol{n}}$. To show this, let ρ' be any function which satisfies the constraints, Eq. (4); and, let $u(\hat{\boldsymbol{n}}) = \alpha + \boldsymbol{A}\hat{\boldsymbol{n}}$. Now, we can perturb ρ with some arbitrary function $\delta\rho(\hat{\boldsymbol{n}})$ and still satisfy the constraints provided that

$$\int_{\mathbb{S}^2} \mathrm{d}A\, \delta\rho = 0, \quad \int_{\mathbb{S}^2} \mathrm{d}A\, (\delta\rho)\hat{\boldsymbol{n}} = 0. \qquad [7]$$

Then the change in internal energy due to $\rho \to \rho + \delta\rho$ is

$$\int_{\mathbb{S}^2} \mathrm{d}A\, (\rho + \delta\rho)u - \int_{\mathbb{S}^2} \mathrm{d}A\, \rho u = \int_{\mathbb{S}^2} \mathrm{d}A\, (\delta\rho)(\alpha + \boldsymbol{A}\hat{\boldsymbol{n}})$$

which vanishes by Eq. (7). Therefore, if the monomer potential energy is linear in $\hat{\boldsymbol{n}}$, then all ρ which satisfy Eq. (4) have the same internal energy. In conclusion, we infer that, in this case, the density which minimizes the free energy is the same as that which maximizes the entropy.

Next, using Eq. (6) and Eq. (3) in Eq. (5), we obtain the chain free energy:

$$\mathcal{F} = n\left[\frac{1}{\beta}\left(\gamma\xi + \ln\frac{\xi\operatorname{csch}\xi}{4\pi}\right) - \gamma(\boldsymbol{\mathcal{E}} \cdot \hat{\boldsymbol{r}})\right]. \qquad [8]$$

Finally, we define the chain polarization as $\boldsymbol{p} = \int_{\mathbb{S}^2} \mathrm{d}A\, \rho\boldsymbol{\mu}$. It is easy to show that $-\partial\mathcal{F}/\partial\boldsymbol{E} = \boldsymbol{p}$[§]. Thus,

$$\boldsymbol{p} = \boldsymbol{M}\frac{\boldsymbol{r}}{b} = n\gamma\boldsymbol{M}\hat{\boldsymbol{r}}, \qquad [9]$$

where $\hat{\boldsymbol{r}} = \boldsymbol{r}/r$. By Eq. (9), the chain polarization is determined uniquely by the chain end-to-end vector, irrespective of the temperature or the electric field. In addition, since $\gamma \in [0,1]$ we have that $p \in [0, n\kappa(\boldsymbol{M})]$ where $\kappa(\square)$ is the spectral radius of $\square$. If $\boldsymbol{M} = \mu\boldsymbol{Q}$ then the maximum polarization simplifies to $n\mu$ and occurs when the chain is fully stretched. Importantly, despite the fact that dipole-dipole interactions were assumed negligible in deriving Eq. (9), we note that Markov chain Monte Carlo simulations agree with Eq. (9) nearly exactly, even when dipole-dipole interactions *are* significant (see §1 of the SI).

3. Statistical mechanics of the electroelasticity of a wormlike chain

Ultimately, because we are interested in what universal phenomena may arise from all polymer chains with polar monomers–not just those that behave as freely jointed chains– we next consider polar monomers in a wormlike chain. By wormlike chain, we mean a chain which again consists of rigid monomers but has some bending stiffness along its contour. That is, the bond which joins monomer i to monomer $i+1$ has rotational stiffness K_i. Recalling $\boldsymbol{\mathcal{E}} := \boldsymbol{M}^T\boldsymbol{E}$, the Hamiltonian reads:

$$\mathcal{H} = \sum_{i=1}^{n} \left(\frac{K_i}{2b}(\hat{\boldsymbol{n}}_{i+1} - \hat{\boldsymbol{n}}_i)^2 - \boldsymbol{\mathcal{E}} \cdot \hat{\boldsymbol{n}}_i \right). \qquad [10]$$

where it is assumed that $K_n = 0$ to simulate a hinged boundary condition (at the chain's end). In the limit of $b \to 0$ and $n \to \infty$, Eq. (10) becomes:

$$\mathcal{H} \simeq \int_0^L \left(\frac{K(s)}{2} \left| \frac{d\hat{\boldsymbol{n}}}{ds} \right|^2 - \frac{1}{b}\boldsymbol{\mathcal{E}} \cdot \hat{\boldsymbol{n}} \right) ds, \qquad [11]$$

where $L = nb$ is the chain length and the chain is parameterized by its arclength, $s \in [0, L]$. For simplicity we assume that the stiffness is same throughout the chain, i.e. $K(s) = K$.

Here we again consider a fixed end-to-end vector ensemble. Formally, the end-to-end vector and normalization constraints are:

$$\boldsymbol{g}[\hat{\boldsymbol{n}}] = \frac{1}{L} \left(b\sum_{i=1}^{n} \hat{\boldsymbol{n}}_i - \boldsymbol{r} \right) \simeq \frac{1}{L} \int_s \hat{\boldsymbol{n}}\, ds - \frac{\boldsymbol{r}}{L} = \boldsymbol{0}, \qquad [12]$$

$$h(s) = \hat{\boldsymbol{n}}_i \cdot \hat{\boldsymbol{n}}_i - 1 \simeq \hat{\boldsymbol{n}}(s) \cdot \hat{\boldsymbol{n}}(s) - 1 = 0.$$

Let $\boldsymbol{g}[\hat{\boldsymbol{n}}] = (g_1, g_2, g_3)$, when evaluating the partition function, the constraints are enforced through Dirac delta distributions (84) and functionals (85):

$$\mathcal{Z} = \int \exp[-\beta\mathcal{H}]\, \delta(g_1)\delta(g_2)\delta(g_3)\delta[h]\, \mathcal{D}\hat{\boldsymbol{n}}.$$

Using the Fourier space representations of the Dirac delta distributions and functional (85), we have:

$$\mathcal{Z} = \frac{1}{(2\pi)^4} \int \exp\left[-\beta\mathcal{H}^{\text{eff}}\right]\, d^3\boldsymbol{k}\, \mathcal{D}\gamma\, \mathcal{D}\hat{\boldsymbol{n}}, \qquad [13]$$

where $\boldsymbol{k} = \{k_1, k_2, k_3\}$ and $\gamma = \gamma(s)$ are wave vectors; and where the effective Hamiltonian is defined as:

$$\mathcal{H}^{\text{eff}} \simeq \int_0^L \left(\frac{K}{2} \left| \frac{d\hat{\boldsymbol{n}}}{ds} \right|^2 - \frac{1}{b}\boldsymbol{\mathcal{E}} \cdot \hat{\boldsymbol{n}} - \frac{i}{L\beta}\boldsymbol{k} \cdot \hat{\boldsymbol{n}} \right) ds$$
$$+ \frac{i}{L\beta}\boldsymbol{k} \cdot \boldsymbol{r} - \int_0^L \frac{i}{L\beta}\gamma(s)(\hat{\boldsymbol{n}} \cdot \hat{\boldsymbol{n}} - 1)\, ds. \qquad [14]$$

The last term in Eq. (14) is anharmonic, and therefore makes Eq. (13) difficult, if not impossible, to evaluate exactly. As a result, we proceed to approximate the partition function by dropping the normalization constraint, i.e. we let $\gamma(s) \to 0$. This elimination is equivalent to allowing the monomers to stretch or contract. We show in §2 of the SI, by using a variational approach, that this assumption (interestingly) does not alter our result.

Next to evaluate (the harmonic approximation of) $\mathcal{Z}$, we use the Fourier transform of $\hat{\boldsymbol{n}}(s)$ given by:

$$\hat{\boldsymbol{n}}(s) = \sum_{q \in \mathbb{K}} \boldsymbol{\omega}(q) \exp[iqs], \qquad [15]$$

where $\mathbb{K} = \{q : q = 2n\pi/L, n \in \mathbb{Z}, q_{min} \le |q| \le q_{max}\}$ and $q_{min} = 0$ and $q_{max} = 2\pi/b$. The amplitudes of each mode $\boldsymbol{\omega}(q)$ can be achieved by:

$$\boldsymbol{\omega}(q) = \frac{1}{L} \int_0^L \hat{\boldsymbol{n}}(s) \exp[-iqs] ds. \qquad [16]$$

By definitions Eq. (15) and Eq. (16), we rewrite the effective Hamiltonian in Eq. (14) as follows:

$$\mathcal{H}_0^{\text{eff}} = L\sum_{q \in \mathbb{K}} \left(\frac{K}{2}q^2 |\boldsymbol{\omega}(q)|^2 \right) - \frac{L}{b}\boldsymbol{\mathcal{E}} \cdot \boldsymbol{\omega}(0)$$
$$- \frac{i}{\beta}\boldsymbol{k} \cdot \boldsymbol{\omega}(0) + \frac{i}{L\beta}\boldsymbol{k} \cdot \boldsymbol{r}, \qquad [17]$$

where $\mathcal{H}_0^{\text{eff}}$ is the effective Hamiltonian upon dropping the normalization constraint, and $\boldsymbol{\omega}(0) = \boldsymbol{r}/L$ by definition. Notice that the partition function is now harmonic in the unknowns. Indeed, introducing $\boldsymbol{\alpha}(q, k) = [\omega_1(q_{min} : q_{max}), \omega_2(q_{min} : q_{max}), \omega_3(q_{min} : q_{max}), k_1, k_2, k_3]$ where $\text{Size}(\boldsymbol{\alpha}) =: m$, we rewrite Eq. (17) as a quadratic function with the linear term:

$$\beta\mathcal{H}_0^{\text{eff}} = \sum_{i,j=1}^{m} \frac{1}{2}\alpha_i A_{ij}\alpha_j + b_i\alpha_i, \qquad [18]$$

where $\boldsymbol{A}$ and $\boldsymbol{b}$ can be achieved from Eq. (17) by straight forward calculation. Plugging Eq. (18) into Eq. (13):

$$\mathcal{Z}_0 = \frac{1}{(2\pi)^4} \int \exp\left[-\beta\mathcal{H}_0^{\text{eff}}\right] d^m\boldsymbol{\alpha},$$
$$= \frac{1}{(2\pi)^4} \sqrt{\frac{(2\pi)^m}{\prod_{|q| \in \mathbb{K}\&q\neq0}(2L\beta K|q|^2)^3}} \exp\left[\frac{\beta}{b}\boldsymbol{\mathcal{E}} \cdot \boldsymbol{r}\right]. \qquad [19]$$

Once the partition function is obtained, we can identify the free energy of the system as follows:

$$\mathcal{F} = -\frac{1}{\beta}\ln(\mathcal{Z}_0) = \text{const} + \frac{3}{2\beta}\sum_{|q| \in \mathbb{K}\&q\neq0}\ln(2L\beta K|q|^2) - \frac{1}{b}\boldsymbol{\mathcal{E}} \cdot \boldsymbol{r}$$

Thus recalling $\boldsymbol{\mathcal{E}} := \boldsymbol{M}^T\boldsymbol{E}$, by definition, the polarization can be achieved by

$$\boldsymbol{p} = -\frac{\partial\mathcal{F}}{\partial\boldsymbol{E}} = \boldsymbol{M}\frac{\boldsymbol{r}}{b} = n\gamma\boldsymbol{M}\hat{\boldsymbol{r}}, \qquad [20]$$

which is identical to Eq. (9). We remark, as already noted earlier, that accounting for normalization constraint, does not

change the polarization of the system.

In the remainder of the work, we show that the stretch-polarization relationship (i.e. the relationship between a chain's end-to-end vector and its net dipole) is a key component to the flexoelectric effect of elastomers consisting of polar monomers. By Eq. (9) and Eq. (20), we can see that this relationship is consistent for both freely jointed and wormlike chains, and is invariant with respect to the ambient temperature or applied electric field. Further, although the analytical expressions were determined by assuming negligible dipole-dipole interactions, Monte Carlo simulations agree nearly exactly, even when dipole-dipole interactions are significant (SI). This surprisingly consistent result is a consequence of the monomer dipole constitutive response and the correspondence between thermodynamic state variables and ensemble averages. Indeed, let $\langle \square \rangle$ denote the ensemble average of $\square$. Then, the same relationship can be obtained almost by definition:

$$\boldsymbol{r} = b \left\langle \sum_{i=1}^{n} \hat{\boldsymbol{n}}_i \right\rangle,$$

$$\boldsymbol{p} = \left\langle \sum_{i=1}^{n} \boldsymbol{\mu}_i \right\rangle = M \left\langle \sum_{i=1}^{n} \hat{\boldsymbol{n}}_i \right\rangle = M \frac{\boldsymbol{r}}{b}.$$

The broad applicability of the monomer dipole constitutive model (i.e. dipolar molecules are not uncommon (86)) and the consistency of the stretch-polarization relationship together suggest that the theory developed herein is potentially quite general; that is, it is expected to be valid for a wide range of types of elastomers, and for a variety of loading and environmental conditions.

4. Network polarization: coarse-graining from chain-scale to the continuum scale

In coarse-graining from the chain scale to the continuum scale, we assume that each material point can be represented by a probability distribution of chains and that these chains are in weak interaction with each other (that is, the free energy density at a material point is approximately the product of the average chain free energy–as if the chains were in isolation–and the density of chains per unit volume (87)). This assumption is standard in elastomer elasticity (75, 78, 88–90), and has been used recently in elastomer electroelastictiy (79–81, 91). It is also consistent with our assumption that monomer-monomer interactions are negligible within a chain itself. Let $\langle \square \rangle_{\boldsymbol{r}}$ denote the average of $\square$ over chains in the current configuration. Then, by the weak interaction assumption, the closed-dielectric free energy density, $\mathcal{W}^*$, at a material point is

$$\mathcal{W}^* = N \langle \mathcal{F} \rangle_{\boldsymbol{r}}, \qquad [21]$$

where N is the number of chains per unit volume. Similarly, we take the (continuum-scale) polarization (i.e. dipole moment per unit volume), $\boldsymbol{P}$, as the average over chain polarizations; that is

$$\boldsymbol{P} = N \langle \boldsymbol{p} \rangle_{\boldsymbol{r}} = N M \left\langle \frac{\boldsymbol{r}}{b} \right\rangle_{\boldsymbol{r}}. \qquad [22]$$

Note that, as a consequence of Eq. (5) and Eq. (22), and since averaging is a linear operation: $\boldsymbol{P} = -\partial \mathcal{W}^* / \partial \boldsymbol{E}$ [¶]. This result,

in congruence with a rigorous thermodynamic treatment of the consequences of deriving the chain scale free energy in a fixed electric field ensemble, leads us to the conclusion that $\mathcal{W}^*$ is the Legendre transform (with respect to polarization) of the Helmholtz free energy density, $\mathcal{W}$. Thus,

$$\mathcal{W} = \mathcal{W}^* - \boldsymbol{P} \cdot \boldsymbol{E}. \qquad [23]$$

The chain averaging considered thus far has been in the current configuration. To instead understand these quantities in terms of the reference configuration and continuum-scale deformations, we must make a kinematic assumption regarding how chains in the reference configuration are mapped into the current configuration[‖]. Here we assume that chain end-to-end vectors are mapped from the reference to the current configuration under the deformation gradient, $\boldsymbol{F}$. In the literature, this is known as the *affine deformation assumption* (75).

Finally, let $\langle \square \rangle_{\tilde{\boldsymbol{r}}}$ denote the average of $\square$ over chains in the reference configuration, $J := \det \boldsymbol{F}$, $N_0 := JN$ and $\tilde{\boldsymbol{P}} := J\boldsymbol{P}$. (We say that $\tilde{\boldsymbol{P}}$ is the pullback of $\boldsymbol{P}$.) Then

$$\mathcal{W}^* \left(\boldsymbol{F}; \boldsymbol{E} \right) = N_0 \left\langle \mathcal{F} \left(\boldsymbol{F}\tilde{\boldsymbol{r}}, \boldsymbol{E} \right) \right\rangle_{\tilde{\boldsymbol{r}}},$$

$$\mathcal{W} \left(\boldsymbol{F}; \boldsymbol{E} \right) = \mathcal{W}^* \left(\boldsymbol{F}, \boldsymbol{E} \right) - J^{-1} \tilde{\boldsymbol{P}} \left(\boldsymbol{F} \right) \cdot \boldsymbol{E},$$

$$\tilde{\boldsymbol{P}} \left(\boldsymbol{F} \right) = N_0 \left\langle \boldsymbol{p} \left(\boldsymbol{F}\tilde{\boldsymbol{r}} \right) \right\rangle_{\tilde{\boldsymbol{r}}},$$

where we write $\tilde{\boldsymbol{P}} = \tilde{\boldsymbol{P}} \left(\boldsymbol{F} \right)$ to reinforce the fact that, in the case when monomer-monomer and chain-chain interactions are negligible, the polarization is determined uniquely by the deformation. We also mention that $\boldsymbol{E}$ is not a freely varying parameter but is determined from Gauss's law; that is,

$$\operatorname{div} \boldsymbol{E} = \frac{1}{\epsilon_0} \left(\varrho_f - \operatorname{div} \boldsymbol{P} \right),$$

where ϵ_0 is the permittivity of free space and ϱ_f is the density of free charges.

Before moving on, we pause to consider $\tilde{\boldsymbol{P}}$. It is certainly true for an isotropic distribution of chains, but–since polymer chains are essentially entropic springs with a minimum energy length of $r = 0$–even for a general stress-free distribution of chains, we expect that $\langle \tilde{\boldsymbol{r}} \rangle_{\tilde{\boldsymbol{r}}} = 0$. For any such reference distribution of chains, we find that, under the affine deformation assumption, the polarization vanishes for all $\boldsymbol{F}$. Indeed, since averaging is linear,

$$\tilde{\boldsymbol{P}} = N_0 \left\langle M \frac{\boldsymbol{F}\tilde{\boldsymbol{r}}}{b} \right\rangle_{\tilde{\boldsymbol{r}}} = \frac{N_0}{b} M \boldsymbol{F} \langle \tilde{\boldsymbol{r}} \rangle_{\tilde{\boldsymbol{r}}} = \boldsymbol{0}.$$

It would seem then that our model, at least thus far, is not very interesting. More precisely, this model does not give rise to *piezoelectricity*. This is also reassuring in a sense that a conventional elastomer is indeed not piezoelectric, however, we will (in due course) aside from flexoelectricity, be able to comment on the precise conditions for the design of emergent piezoelectricity as well.

[¶] This follows, in part, because their nonlocal relationship at the chain-scale simplifies to a local one (81).

[‖] Historically, there has been some controversy related to this. The two most common kinematic assumptions are what we will refer to as the *affine deformation assumption* and the *cooperative network assumption*. In either case, the reference chains are arranged in a unit cell and the cell is deformed in relation to the deformation gradient, $\boldsymbol{F}$. According to the affine deformation assumption, the chain end-to-end vectors in the reference configuration, $\tilde{\boldsymbol{r}}$, are mapped to the current configuration by $\boldsymbol{r} = \boldsymbol{F}\tilde{\boldsymbol{r}}$ (75); where as, for the cooperative network assumption, the unit cell is first rotated such that its axes are aligned with the principal frame (77). Then the cell is deformed along each of its axes according to its respective principal stretch. In both the context of elasticity (75, 78) and electroelasticity (92, 93), there are important differences between the two assumptions and can sometimes even lead to qualitatively different behaviors. In this work, we will focus on deformations which, in the frame of reference of interest, is such that $\boldsymbol{F}$ is diagonal. Thus, the two kinematic assumptions will be equivalent.
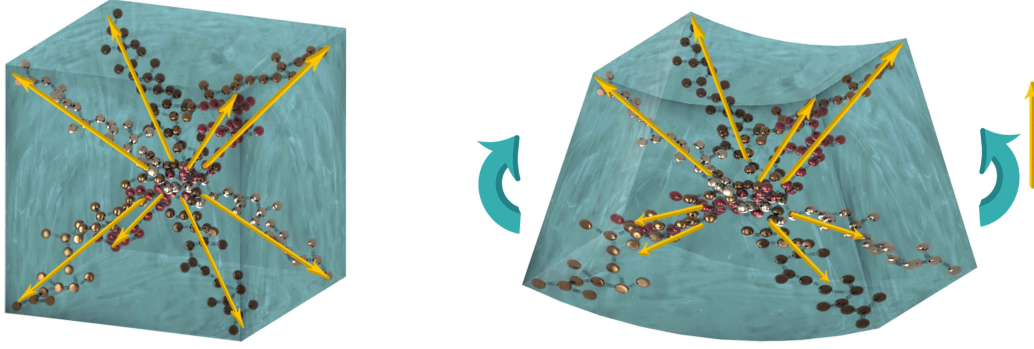
Fig. 2. Schematic of a unit cell of an 8-chain model in (a) reference and (b) deformed state upon bending. The yellow arrows indicate the chain polarization in both configurations. While the unit cell in reference configuration is electrically neutral, the net polarization is upward in the deformed configuration under bending.

5. Flexoelectricity and the elastomer unit cell

Moving forward, we will be interested in the polarization as a function of Grad $\boldsymbol{F}$ where $\boldsymbol{F}$ is the deformation gradient; that is, we are interested in $\tilde{\boldsymbol{P}} = \tilde{\boldsymbol{P}}(\text{Grad } \boldsymbol{F})$ and whether or not this relationship is as trivial as the polarization as a function of merely $\boldsymbol{F}$. The Grad $\boldsymbol{F}$ term could, for instance, be the result of a bending deformation and, hence, result in flexoelectricity. To model the effects of Grad $\boldsymbol{F}$ at a material point, we must now think beyond the probability distribution of $\tilde{r}$ and consider also the geometry of the unit cell.

Prior work (mentioned in the previous section (75, 77, 88–90)) which developed and made use of a unit cell in the reference configuration in order to relate continuum-scale deformations to chain-scale deformations were focused primarily on the statistical distribution of chain end-to-end vectors and the choice of kinematic assumption. To the authors' knowledge, the geometry of the unit cell was not ever considered significant in and of itself (other than to ensure that $\tilde{r} = b\sqrt{n}$ for all $\tilde{r}$). We are therefore in the position of being interested in defining a unit cell geometry but of being more or less without precedent. Therefore, as a first example, we will assign dimensions to the Arruda-Boyce 8-chain model (or rather, determine the dimensions and let them, for the first time, have physical significance) (see (77, 78) for example). The unit cell Fig. 2(a) consists of eight chains, each emanating from the center of the cell to one of the eight corners of the cube.

Each chain is assumed to satisfy $\tilde{r} = b\sqrt{n}$ [**]; thus, the length of an edge of the unit cell is $\ell := 2b\sqrt{n/3}$. The kinematic assumption that we now make–similar to the affine deformation assumption–will be that 1) the unit cell deforms under $\boldsymbol{F}$ (where $\boldsymbol{F}$ is allowed to vary throughout the cell) and 2) the beginning and end of the chain end-to-end vectors remain rigidly attached to their corresponding points in the unit cell. For the 8-chain model, this means that each of the end-to-end vectors, in the deformed configuration, still begins at the center of the cell and ends at its respective corner.

[**] The length $b\sqrt{n}$ is motivated by random walk statistics. It is the most likely distance (from the starting point) for a random walk of n steps with step length b. Assuming all chains in the reference configuration have length $\tilde{r} = b\sqrt{n}$ is a standard assumption in the constitutive modeling of rubber (75, 77, 88–90).

Having decided on an example unit cell, we next identify deformations of interest. As mentioned previously, we will limit our investigation, for the time being, to diagonal $\boldsymbol{F}$. In addition, since most elastomers are approximately incompressible, we will consider $\boldsymbol{F}$ such that $J = 1$. Thus, let

$$\boldsymbol{F}(\boldsymbol{x}) = \text{diag}\left(\lambda_1(\boldsymbol{x}), \lambda_2(\boldsymbol{x}), (\lambda_1(\boldsymbol{x})\lambda_2(\boldsymbol{x}))^{-1}\right), \quad [24]$$

where $\boldsymbol{x}$ is the position of a material point in the reference configuration. For ease of notation, let $\lambda_{i,j} := \partial\lambda_i/\partial x_j$. Then, we assume $\boldsymbol{F}$ varies gradually enough relative to the size of a unit cell such that Grad $\boldsymbol{F}$ is approximately constant. To be precise, we assume $\epsilon := \max_{i,j}|\tilde{r}\lambda_{i,j}| \ll 1$. Next let $\boldsymbol{y}$ denote a position within the 8-chain unit cell so that $y_i \in [x_i - \ell/2, x_i + \ell/2]$. Then, $\lambda_i(\boldsymbol{y}) = \lambda_i(\boldsymbol{x}) + \sum_{j=1}^{3}\lambda_{i,j}(\boldsymbol{x})y_j + \mathcal{O}(\epsilon^2)$. Neglecting $\mathcal{O}(\epsilon^2)$ terms, we have the result:

$$\langle\boldsymbol{r}\rangle_{\boldsymbol{r}} = \frac{\tilde{r}}{3}(\tilde{r}\lambda_{1,1}, \tilde{r}\lambda_{2,2}, \alpha_3), \quad [25]$$

where

$$\alpha_3 = \frac{\sqrt{3}}{8}\sum_{i=1}^{2}\sum_{j=1}^{2}\sum_{k=1}^{2}\left\{(-1)^k\right.$$

$$\times\left[\lambda_1 + \frac{\tilde{r}}{\sqrt{3}}\left((-1)^i\lambda_{1,1} + (-1)^j\lambda_{1,2} + (-1)^k\lambda_{1,3}\right)\right]^{-1}$$

$$\left.\times\left[\lambda_2 + \frac{\tilde{r}}{\sqrt{3}}\left((-1)^i\lambda_{2,1} + (-1)^j\lambda_{2,2} + (-1)^k\lambda_{2,3}\right)\right]^{-1}\right\}$$

The expression for α_3 is still complicated however. To simplify further, and because we are ultimately interested in flexoelectricity, consider λ_1 and λ_2 of the form:

$$\lambda_j = \overline{\lambda}_j + \lambda_{j,3}x_3, \quad [26]$$

as this could correspond to a bending about some axis in the $\hat{\boldsymbol{e}}_1, \hat{\boldsymbol{e}}_2$ plane. In this case,

$$\langle\boldsymbol{r}\rangle_{\boldsymbol{r}} = \left(0, 0, \frac{-3\tilde{r}^2\left(\overline{\lambda}_2\lambda_{1,3} + \overline{\lambda}_1\lambda_{2,3}\right)}{\left(3\overline{\lambda}_1^2 - \tilde{r}^2\lambda_{1,3}^2\right)\left(3\overline{\lambda}_2^2 - \tilde{r}^2\lambda_{2,3}^2\right)}\right), \quad [27]$$

such that, in general, we have a nonzero polarization. Further, we can see from Eq. (22) that if $\boldsymbol{M} = \mu\boldsymbol{I}$ (where $\boldsymbol{I}$ is the
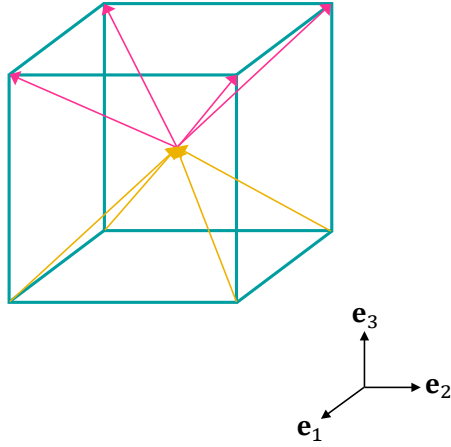
Fig. 3. Schematic of an eight-chain model exhibiting piezoelectric behavior. The arrows show the direction of the polarization of each chain.

identity operator) then $\boldsymbol{P}$ is aligned (or anti-aligned) with $\mathrm{Grad}\,\lambda_1$ and $\mathrm{Grad}\,\lambda_2$ (i.e. the $\hat{\boldsymbol{e}}_3$ direction).

We can make the following observations regarding Eq. (27):

- It is interesting to see in Eq. (27) that $\langle r \rangle_{\boldsymbol{r}}$ can diverge if $3\overline{\lambda}_1{}^2 = \tilde{r}^2\lambda_{1,3}^2$ or $3\overline{\lambda}_2{}^2 = \tilde{r}^2\lambda_{2,3}^2$. For this to occur, roughly speaking, the deformation gradient $\boldsymbol{F}$ must change appreciably relative to the size of the unit cell (more precisely, $\tilde{r}\lambda_{i,3} = \mathcal{O}(1)$). This violates a prior assumption and so it should not be surprising that it leads to nonphysical results. If $\boldsymbol{F}$ changes appreciably relative to size of the unit cell then perhaps our unit cell is too large or we need to resort to a different modeling approach altogether.

- It is also interesting that if $\overline{\lambda}_2\lambda_{1,3} = -\overline{\lambda}_1\lambda_{2,3}$ then $\tilde{\boldsymbol{P}}$ vanishes. This is, in part, because of incompressibility. Indeed, let λ_3 denote the stretch in the $\hat{\boldsymbol{e}}_3$ direction. Then,

$$\lambda_3 = \left(\overline{\lambda}_1\overline{\lambda}_2 + \left(\overline{\lambda}_2\lambda_{1,3} + \overline{\lambda}_1\lambda_{2,3} \right) x_3 + \lambda_{1,3}\lambda_{2,3}x_3^2 \right)^{-1},$$

such that $\left(\overline{\lambda}_2\lambda_{1,3} + \overline{\lambda}_1\lambda_{2,3} \right) = 0$ implies $\lambda_3(x_3)$ is an even function; and therefore all of the chains experience the same stretch in the $\hat{\boldsymbol{e}}_3$ direction.

- To see how the flexoelectric effect scales with stretch, consider $\overline{\lambda}_3 := \left(\overline{\lambda}_1\overline{\lambda}_2 \right)^{-1}$. Neglecting $\mathcal{O}\left(\epsilon^2\right)$ terms in the denominator of Eq. (27) results in $\tilde{P}_3 \sim \mathcal{O}\left(\left(\overline{\lambda}_2\lambda_{1,3} + \overline{\lambda}_1\lambda_{2,3} \right) \overline{\lambda}_3^2 \right)$. As a result, we see that our theory agrees with the surprising experimental result that pre-stretching the elastomer in the direction of $\mathrm{Grad}\,\boldsymbol{F}$ can lead to giant flexoelectricity (94). Note that if $\overline{\lambda}_1 = \overline{\lambda}_2 = \overline{\lambda}_3^{-1/2}$ then this enhancement scales as $\overline{\lambda}_3^{3/2}$; however, if $1 = \overline{\lambda}_1 \gg \overline{\lambda}_2 = \overline{\lambda}_3^{-1}$ (or vice versa) then *the enhancement is quadratic in* $\overline{\lambda}_3$.

6. Elastomer design and the conditions for the *piezoelectric* effect

Although not the primary focus of the current work, since piezoelectricity is arguably the most well-known and direct form of electromechanical coupling, it would be illuminating

to understand the precise conditions under which an elastomer can be designed to exhibit such a property. We emphasize once again that while flexoelectricity is universal, piezoelectricity is not and we know of no piezoelectric elastomers[††]. To make progress on this, we assume that $\boldsymbol{M}$ differs from chain to chain. By doing so, from Eq. (22) the polarization becomes:

$$\tilde{\boldsymbol{P}} = J\boldsymbol{P} = JN\langle \boldsymbol{p} \rangle_{\boldsymbol{r}} = N_0 \left\langle \boldsymbol{M}\frac{\boldsymbol{r}}{b} \right\rangle_{\boldsymbol{r}}. \qquad [28]$$

A special case can be constructed by considering a relation of $\boldsymbol{M}^{(2)} = -\boldsymbol{M}^{(1)}$ in which $\boldsymbol{M}^{(1)}(\boldsymbol{M}^{(2)})$ belongs to the upper(lower) half chains in $\hat{\boldsymbol{e}}_3$ direction of the eight chain model as shown in Fig 3.

Here, by considering the eight chain model, we are assuming that the system is isotropic from a mechanical (elastic) perspective, while the linear transformation $\boldsymbol{M}$ is not unique in the entire cell and thus not isotropic from an electrostatic point of view. This assumption gives us a nonvanishing polarization, even in the reference configuration.

We consider a deformation which varies along the unit cell i.e. $\lambda_i(\boldsymbol{y}) = \lambda_i(\boldsymbol{x}) + \sum_{j=1}^3 \lambda_{i,j}(\boldsymbol{x})y_j + \mathcal{O}\left(\epsilon^2\right)$. Based on the model we introduced for flexoelectricity in previous section, we obtain:

$$\langle \boldsymbol{M}\boldsymbol{r} \rangle_{\boldsymbol{r}} = \frac{1}{2}\left[\langle \boldsymbol{M}^{(1)}\boldsymbol{r} \rangle_{\boldsymbol{r}} + \langle \boldsymbol{M}^{(2)}\boldsymbol{r} \rangle_{\boldsymbol{r}} \right]$$
$$= \boldsymbol{M}^{(1)}\frac{\tilde{r}}{3}(0,0,\alpha_3),$$

where

$$\alpha_3 = \frac{\sqrt{3}}{8}\sum_{i=1}^2\sum_{j=1}^2\sum_{k=1}^2$$

$$\left\{ \left[\lambda_1 + \frac{\tilde{r}}{\sqrt{3}}\left((-1)^i\lambda_{1,1} + (-1)^j\lambda_{1,2} + (-1)^k\lambda_{1,3} \right) \right]^{-1} \right.$$

$$\left. \times \left[\lambda_2 + \frac{\tilde{r}}{\sqrt{3}}\left((-1)^i\lambda_{2,1} + (-1)^j\lambda_{2,2} + (-1)^k\lambda_{2,3} \right) \right]^{-1} \right\}.$$

Again, our ultimate goal is to investigate flexoelectricity. Therefore, restricting our attention to the bending about some axis in the $\hat{\boldsymbol{e}}_1, \hat{\boldsymbol{e}}_2$ plane same as Eq. (26), we obtain the net polarization after the deformation of the unit cell as follows:

$$\tilde{\boldsymbol{P}} = N_0 \left\langle \boldsymbol{M}\frac{\boldsymbol{r}}{b} \right\rangle_{\boldsymbol{r}}$$

$$= N_0\boldsymbol{M}^{(1)}\left(0, 0, \frac{\sqrt{3}\tilde{r}\left(3\overline{\lambda}_1\overline{\lambda}_2 + \tilde{r}^2\lambda_{1,3}\lambda_{2,3} \right)}{\left(3\overline{\lambda}_1{}^2 - \tilde{r}^2\lambda_{1,3}^2 \right)\left(3\overline{\lambda}_2{}^2 - \tilde{r}^2\lambda_{2,3}^2 \right)} \right)^T.$$

Here, there are few observations that can be made:

1. The net polarization after the deformation has contributions from two different types of deformations. The first term (in the numerator) is from the deformation gradient itself which is indication of the piezoelectric effect, meanwhile the second term originates from the gradients of the deformation gradient which is indication of the flexoelectric behavior.

[††]Certain polymers–but not elastomers–do exhibit piezoelectricity such as polyvinylidene difluoride(PVDF) (95) and of polymer-ceramic composites (96).

2. By assumption, $\max_j |\tilde{r}\lambda_{j,3}| = \mathcal{O}(\epsilon)$ is small. Thus, the second term, which is attributed to the flexoelectric effect, is much smaller than the flexoelectric response of the electrically isotropic case in previous section (to be precise, it is $\mathcal{O}(\epsilon^2)$ compared to $\mathcal{O}(\epsilon)$). The conclusion is that, in this case, while we have increased the piezoelectric effect, it has been at the expense of flexoelectricity.

3. Similar to the previous setup of the unit cell, stretching the unit cell in $\hat{e}_3$ direction, can enhance both piezoelectric and flexoelectric response in a linear and quadratic way respectively.

7. The design of elastomers for emergent flexoelectricity

Clearly, we should maximize the spectral radius of $\boldsymbol{M}$ if we aim to maximize the flexoelectric effect. For the case of a fixed dipole rigidly attached to each monomer (i.e. $\boldsymbol{M} = \mu\boldsymbol{Q}$), this amounts to maximizing the magnitude of the dipoles, μ. We could potentially engage in such a design process (computationally) by using density functional theory (see (97), for example). However, we also note that it is often trivial to increase the density of cross-links in an elastomer. In addition, we could theoretically influence the alignment of chains in the network by weakly cross-linking, applying an external electric field, and then cross-linking further. Therefore, it is also conceivable that the unit cell itself be taken as a design variable (see (81)). This may prove to be a fruitful endeavor since, for elastomers that consist of the type of polymer chains considered herein, the geometry of the unit cell and the arrangement of chains within the unit cell influence the magnitude and direction of the flexoelectric effect.

The main goal that we now focus on is to design an elastomer unit cell to tune the flexoelectric response. In particular, we propose that (in analogy with the dominant role a dipole moment plays in the phenomenon of piezoelectricity) that flexoelectricity is primarily dictated by the next-order multipole expansion term–the quadrupolar moment. In particular, we anticipate unit cells with large variations to have a stronger flexoelectric response. The quadrupole moment can be constructed from two dipole moments in opposite direction . The quadrupole moment($\mathcal{Q}$) is a second order moment of charges and can be formulated as (98)

$$\mathcal{Q} = \sum_{i=1}^{n} \left[3\mathbf{x}_i \otimes \mathbf{x}_i - |\mathbf{x}_i|^2 \mathbb{I} \right] q_i, \qquad [29]$$

where the sum is over all discrete charges(q_i), $\mathbf{x}_i$ is the position vector of the charge q_i and $\mathbb{I}$ is the identity matrix. Analogous to the fact that dipole distribution can be architected to design materials with high piezoelectricity, quadrupole moment and its gradient can play the same role in designing giant flexoelectric materials.

Here we aim to establish a reference unit cell with vanishing net polarization but finite quadrupole moment and its gradient. The authors claim that the higher gradient in quadrupole moment will result in higher flexoelectric effect. The simplest example can be achieved by enforcing an inversion symmetry about the center of the 8-chain unit cell, (as shown in Fig. 4)
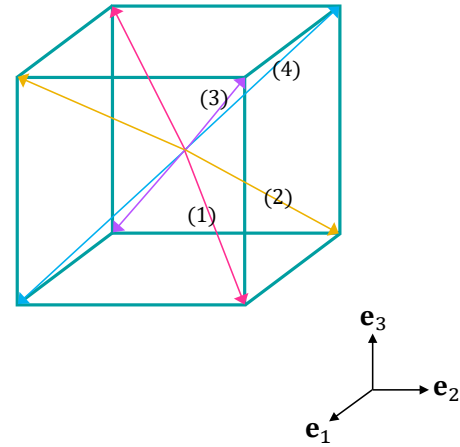

Fig. 4. Design of an eight-chain unit cell to tune the flexoelectric response. Polymers are paired together through an inversion symmetry as shown by numbers; and, when the electrical properties of the four pairs are tuned to maximize the gradient of the quadruple moment of the unit cell, the flexoelectric response is stretch-invariant.

which leaves four pairs of chains each with a different $\boldsymbol{M}$ and each acting as a quadrupole moment.

We make the choice:

$$\boldsymbol{M} = \frac{1}{K_1}\boldsymbol{M}^{(1)} = \frac{1}{K_2}\boldsymbol{M}^{(2)} = \frac{1}{K_3}\boldsymbol{M}^{(3)} = \frac{1}{K_4}\boldsymbol{M}^{(4)},$$

where, $K_i(i = 1:4)$ are some arbitrary real numbers. Again consider a deformation gradient of the form Eq. (24) and its associated assumptions. By restricting the deformation to the bending of the unit cell similar to Eq. (26), the polarization after the deformation is obtained as:

$$\tilde{\boldsymbol{P}} = \sum_i \frac{N_0^{(i)}}{b} \left\langle \boldsymbol{M}^{(i)} r^{(i)} \right\rangle_{\boldsymbol{r}} = \frac{N_0}{b} \boldsymbol{M}^{(1)} \tilde{r}^2 (\alpha_1, \alpha_2, \alpha_3),$$

where α_i are defined as:

$$\alpha_1 = \frac{1}{12}(K_2 + K_3 - K_1 - K_4)\lambda_{1,3},$$

$$\alpha_2 = \frac{1}{12}(K_3 + K_4 - K_1 - K_2)\lambda_{2,3},$$

$$\alpha_3 = \frac{-3(K_1 + K_2 + K_3 + K_4)\left(\overline{\lambda}_2\lambda_{1,3} + \overline{\lambda}_1\lambda_{2,3}\right)}{4\left(3\overline{\lambda}_1^2 - \tilde{r}^2\lambda_{1,3}^2\right)\left(3\overline{\lambda}_2^2 - \tilde{r}^2\lambda_{2,3}^2\right)}.$$

Upon a closer examination, we notice that the third term is exactly the flexoelectricity constant we obtained in Eq. (27) for the case $K_1 = K_2 = K_3 = K_4 = 1$, which is equivalent to the electrically isotropic case.

However, if we allow the K_i to vary, we see that we can obtain flexoelectricity in the plane orthogonal to $\hat{e}_3$. Indeed, if we make the choice is $K_1 = K_4 = -K_2 = -K_3$, this results in enhancing the α_1 while eliminating α_3. Interestingly, we see that, in this case, the flexoelectric effect is invariant with respect to $\overline{\lambda}_1$ and $\overline{\lambda}_2$. This property may be particularly useful for applications in soft sensors and robotics where we may expect finite stretches to occur but would prefer the flexoelectric response to remain constant, or, at the very least, not diminish.

8. Concluding remarks

In this work, we have established the mechanisms (and the underlying theory) underpinning flexoelectricity in elastomers. Surprisingly, our theory shows that giant flexoelectricity can be attained in incompressible elastomers by pre-stretching the material in the strain gradient direction. In particular, the scaling of the flexoelectric effect with respect to pre-stretch is at least super-linear (with exponent 3/2) and, for certain loading conditions, can scale quadratically with pre-stretch. This suggests a facile route to achieve high-output energy harvesting and high-fidelity soft sensors.

We also considered the design of the polymer network architecture. By poling the chains (e.g. using an applied electric field), we can develop a piezoelectric elastomer. This piezoelectricity is at expense of the flexoelectric effect which diminishes in the poled architecture. The emergent flexoelectric effect can also be (1) made stretch-invariant, and (2) tuned in different directions relative to the direction of the strain gradient by adjusting the quadrupolar moment of the material unit cell. Stretch-invariance may prove useful for soft sensors, and the tunable nature of the flexoelectric direction may be useful for producing soft robots with larger degree of freedom actuators.

1. Christoph Keplinger, Tiefeng Li, Richard Baumgartner, Zhigang Suo, and Siegfried Bauer. Harnessing snap-through instability in soft dielectrics to achieve giant voltage-triggered deformation. *Soft Matter*, 8(2):285–288, 2012.
2. Jeong-Yun Sun, Xuanhe Zhao, Widusha RK Illeperuma, Ovijit Chaudhuri, Kyu Hwan Oh, David J Mooney, Joost J Vlassak, and Zhigang Suo. Highly stretchable and tough hydrogels. *Nature*, 489(7414):133–136, 2012.
3. Jean Won Kwak, Mengdi Han, Zhaoqian Xie, Ha Uk Chung, Jong Yoon Lee, Raudel Avila, Jessica Yohay, Xuexian Chen, Cunman Liang, Manish Patel, et al. Wireless sensors for continuous, multimodal measurements at the skin interface with lower limb prostheses. *Science translational medicine*, 12(574), 2020.
4. John A Rogers, Takao Someya, and Yonggang Huang. Materials and mechanics for stretchable electronics. *science*, 327(5973):1603–1607, 2010.
5. Qian Zhang, Qijie Liang, and John A Rogers. Water-soluble energy harvester as a promising power solution for temporary electronic implants. *APL Materials*, 8(12):120701, 2020.
6. Ruike Zhao, Yoonho Kim, Shawn A Chester, Pradeep Sharma, and Xuanhe Zhao. Mechanics of hard-magnetic soft materials. *Journal of the Mechanics and Physics of Solids*, 124:244–263, 2019.
7. Qiji Ze, Xiao Kuang, Shuai Wu, Janet Wong, S Macrae Montgomery, Rundong Zhang, Joshua M Kovitz, Fengyuan Yang, H Jerry Qi, and Ruike Zhao. Magnetic shape memory polymers with integrated multifunctional shape manipulation. *Advanced Materials*, 32(4):1906657, 2020.
8. Sheng Xu, Yihui Zhang, Lin Jia, Kyle E Mathewson, Kyung-In Jang, Jeonghyun Kim, Haoran Fu, Xian Huang, Pranav Chava, Renhan Wang, et al. Soft microfluidic assemblies of sensors, circuits, and radios for the skin. *Science*, 344(6179):70–74, 2014.
9. Seung-Kyun Kang, Rory KJ Murphy, Suk-Won Hwang, Seung Min Lee, Daniel V Harburg, Neil A Krueger, Jiho Shin, Paul Gamble, Huanyu Cheng, Sooyoun Yu, et al. Bioresorbable silicon electronic sensors for the brain. *Nature*, 530(7588):71–76, 2016.
10. Dae-Hyeong Kim, Shuodao Wang, Hohyun Keum, Roozbeh Ghaffari, Yun-Soung Kim, Hu Tao, Bruce Panilaitis, Ming Li, Zhan Kang, Fiorenzo Omenetto, et al. Thin, flexible sensors and actuators as 'instrumented'surgical sutures for targeted wound monitoring and therapy. *Small*, 8(21):3263–3268, 2012.
11. Dae-Hyeong Kim, Nanshu Lu, Rui Ma, Yun-Soung Kim, Rak-Hwan Kim, Shuodao Wang, Jian Wu, Sang Min Won, Hu Tao, Ahmad Islam, et al. Epidermal electronics. *science*, 333(6044):838–843, 2011.
12. Mengdi Han, Heling Wang, Yiyuan Yang, Cunman Liang, Wubin Bai, Zheng Yan, Haibo Li, Yeguang Xue, Xinlong Wang, Banu Akar, et al. Three-dimensional piezoelectric polymer microsystems for vibrational energy harvesting, robotic interfaces and biomedical implants. *Nature Electronics*, 2(1):26–35, 2019.
13. Alper Erturk and Daniel J Inman. *Piezoelectric energy harvesting*. John Wiley & Sons, 2011.
14. Kewang Nan, Stephen Dongmin Kang, Kan Li, Ki Jun Yu, Feng Zhu, Juntong Wang, Alison C Dunn, Chaoqun Zhou, Zhaoqian Xie, Matthias T Agne, et al. Compliant and stretchable thermoelectric coils for energy harvesting in miniature flexible devices. *Science advances*, 4 (11):eaau5849, 2018.
15. Keun Soo Kim, Yue Zhao, Houk Jang, Sang Yoon Lee, Jong Min Kim, Kwang S Kim, Jong-Hyun Ahn, Philip Kim, Jae-Young Choi, and Byung Hee Hong. Large-scale pattern growth of graphene films for stretchable transparent electrodes. *nature*, 457(7230):706–710, 2009.
16. Dahl-Young Khang, Hanqing Jiang, Young Huang, and John A Rogers. A stretchable form of single-crystal silicon for high-performance electronics on rubber substrates. *Science*, 311 (5758):208–212, 2006.
17. Sheng Xu, Yihui Zhang, Jiung Cho, Juhwan Lee, Xian Huang, Lin Jia, Jonathan A Fan, Yewang Su, Jessica Su, Huigang Zhang, et al. Stretchable batteries with self-similar serpentine interconnects and integrated wireless recharging systems. *Nature communications*, 4(1):1–8, 2013.
18. Yoonho Kim, Hyunwoo Yuk, Ruike Zhao, Shawn A Chester, and Xuanhe Zhao. Printing ferromagnetic domains for untethered fast-transforming soft materials. *Nature*, 558(7709): 274–279, 2018.
19. Kwang J Kim and Satoshi Tadokoro. Electroactive polymers for robotic applications. *Artificial Muscles and Sensors*, 23:291, 2007.
20. Yoonho Kim, German A Parada, Shengduo Liu, and Xuanhe Zhao. Ferromagnetic soft continuum robots. *Science Robotics*, 4(33), 2019.
21. GM Sessler and J Hillenbrand. Electromechanical response of cellular electret films. In *10th International Symposium on Electrets (ISE 10). Proceedings (Cat. No. 99 CH36256)*, pages 261–264. IEEE, 1999.
22. Gerhard Martin Sessler. Physical principles of electrets. In *Electrets*, pages 13–80. Springer, 1980.
23. Michael Wegener and Siegfried Bauer. Microstorms in cellular polymers: A route to soft piezoelectric transducer materials with engineered macroscopic dipoles. *ChemPhysChem*, 6 (6):1014–1025, 2005.
24. Gerda Buchberger, Reinhard Schwödiauer, and Siegfried Bauer. Flexible large area ferroelectret sensors for location sensitive touchpads. *Applied Physics Letters*, 92(12):123511, 2008.
25. Qian Deng, Liping Liu, and Pradeep Sharma. Electrets in soft materials: Nonlinearity, size effects, and giant electromechanical coupling. *Physical Review E*, 90(1):012603, 2014.
26. Liping Liu and Pradeep Sharma. Emergent electromechanical coupling of electrets and some exact relations—the effective properties of soft materials with embedded external charges and dipoles. *Journal of the Mechanics and Physics of Solids*, 112:1–24, 2018.
27. Faezeh Darbaniyan, Kaushik Dayal, Liping Liu, and Pradeep Sharma. Designing soft pyroelectric and electrocaloric materials using electrets. *Soft matter*, 15(2):262–277, 2019.
28. Faezeh Darbaniyan, Kosar Mozaffari, Liping Liu, and Pradeep Sharma. Soft matter mechanics and the mechanisms underpinning the infrared vision of snakes. *Matter*, 4(1):241–252, 2021.
29. Amey Apte, Kosar Mozaffari, Farnaz Safi Samghabadi, Jordan A Hachtel, Long Chang, Sandhya Susarla, Juan Carlos Idrobo, David C Moore, Nicholas R Glavin, Dmitri Litvinov, et al. 2d electrets of ultrathin moo2 with apparent piezoelectricity. *Advanced Materials*, 32(24): 2000006, 2020.
30. Axel Mellinger, Michael Wegener, Werner Wirges, Rajendar Reddy Mallepally, and Reimund Gerhard-Multhaupt. Thermal and temporal stability of ferroelectret films made from cellular polypropylene/air composites. *Ferroelectrics*, 331(1):189–199, 2006.
31. Sana Krichen and Pradeep Sharma. Flexoelectricity: A perspective on an unusual electromechanical coupling. *Journal of Applied Mechanics*, 83(3), 2016.
32. Qian Deng, Liping Liu, and Pradeep Sharma. A continuum theory of flexoelectricity. In *Flexoelectricity in Solids: From Theory to Applications*, pages 111–167. World Scientific, 2017.
33. Thanh D Nguyen, Sheng Mao, Yao-Wen Yeh, Prashant K Purohit, and Michael C McAlpine. Nanoscale flexoelectricity. *Advanced Materials*, 25(7):946–974, 2013.
34. ND Sharma, CM Landis, and P Sharma. Piezoelectric thin-film superlattices without using piezoelectric materials. *Journal of Applied Physics*, 108(2):024304, 2010.
35. J Fousek, LE Cross, and DB Litvin. Possible piezoelectric composites based on the flexoelectric effect. *Materials Letters*, 39(5):287–291, 1999.
36. Baojin Chu, Wenyi Zhu, Nan Li, and L Eric Cross. Flexure mode flexoelectric piezoelectric composites. *Journal of Applied Physics*, 106(10):104109, 2009.
37. Binglei Wang, Shengyou Yang, and Pradeep Sharma. Flexoelectricity as a universal mechanism for energy harvesting from crumpling of thin sheets. *Phys. Rev. B*, 100:035438, Jul 2019. . URL https://link.aps.org/doi/10.1103/PhysRevB.100.035438.
38. Qian Deng, Mejdi Kammoun, Alper Erturk, and Pradeep Sharma. Nanoscale flexoelectric energy harvesting. *International Journal of Solids and Structures*, 51(18):3218–3225, 2014.
39. Xiaoning Jiang, Wenbin Huang, and Shujun Zhang. Flexoelectric nano-generator: Materials, structures and devices. *Nano Energy*, 2(6):1079–1092, 2013.
40. MS Majdoub, P Sharma, and T Çağin. Dramatic enhancement in energy harvesting for a narrow range of dimensions in piezoelectric nanostructures. *Physical Review B*, 78(12):121407, 2008.
41. MS Majdoub, P Sharma, and T Çağin. Erratum: Dramatic enhancement in energy harvesting for a narrow range of dimensions in piezoelectric nanostructures [phys. rev. b 78, 121407 (r)(2008)]. *Physical Review B*, 79(15):159901, 2009.
42. Amir Hossein Rahmati, Siegfried Bauer, and Pradeep Sharma. Nonlinear bending deformation of soft electrets and prospects for engineering flexoelectricity and transverse (d 31) piezoelectricity. *Soft matter*, 15(1):127–148, 2019.
43. Seung-Bok Choi and Gi-Woo Kim. Measurement of flexoelectric response in polyvinylidene fluoride films for piezoelectric vibration energy harvesters. *Journal of Physics D: Applied Physics*, 50(7):075502, 2017.
44. Umesh Kumar Bhaskar, Nirupam Banerjee, Amir Abdollahi, E Solanas, Guus Rijnders, and Gustau Catalan. Flexoelectric mems: towards an electromechanical strain diode. *Nanoscale*, 8(3):1293–1298, 2016.
45. Umesh Kumar Bhaskar, Nirupam Banerjee, Amir Abdollahi, Zhe Wang, Darrell G Schlom, Guus Rijnders, and Gustau Catalan. A flexoelectric microelectromechanical system on silicon. *Nature nanotechnology*, 11(3):263–266, 2016.

46. Zhihong Wang, Xi Xiang Zhang, Xianbin Wang, Weisheng Yue, Jingqi Li, Jianmin Miao, and Weiguang Zhu. Giant flexoelectric polarization in a micromachined ferroelectric diaphragm. *Advanced Functional Materials*, 23(1):124–132, 2013.

47. Amir Abdollahi and Irene Arias. Constructive and destructive interplay between piezoelectricity and flexoelectricity in flexural sensors and actuators. *Journal of Applied Mechanics*, 82 (12), 2015.

48. Qian Deng, Fatemeh Ahmadpoor, William E Brownell, and Pradeep Sharma. The collusion of flexoelectricity and hopf bifurcation in the hearing mechanism. *Journal of the Mechanics and Physics of Solids*, 130:245–261, 2019.

49. WE Brownell, AA Spector, RM Raphael, and Aleksander S Popel. Micro-and nanomechanics of the cochlear outer hair cell. *Annual review of biomedical engineering*, 3(1):169–194, 2001.

50. Kathryn D Breneman, William E Brownell, and Richard D Rabbitt. Hair cell bundles: flexoelectric motors of the inner ear. *PLoS One*, 4(4):e5201, 2009.

51. Qian Deng, Liping Liu, and Pradeep Sharma. Flexoelectricity in soft materials and biological membranes. *Journal of the Mechanics and Physics of Solids*, 62:209–227, 2014.

52. Xin Wen, Dongfan Li, Kai Tan, Qian Deng, and Shengping Shen. Flexoelectret: an electret with a tunable flexoelectriclike response. *Physical review letters*, 122(14):148001, 2019.

53. R Maranganti, ND Sharma, and P Sharma. Electromechanical coupling in nonpiezoelectric materials due to nanoscale nonlocal size effects: Green's function solutions and embedded inclusions. *Physical Review B*, 74(1):014110, 2006.

54. David Codony, Prakhar Gupta, Onofre Marco, and Irene Arias. Modeling flexoelectricity in soft dielectrics at finite deformation. *Journal of the Mechanics and Physics of Solids*, 146: 104182, 2021.

55. Amir Abdollahi, Christian Peco, Daniel Millan, Marino Arroyo, and Irene Arias. Computational evaluation of the flexoelectric effect in dielectric solids. *Journal of Applied Physics*, 116(9): 093502, 2014.

56. Julien Yvonnet and LP Liu. A numerical framework for modeling flexoelectricity and maxwell stress in soft dielectrics at finite strains. *Computer Methods in Applied Mechanics and Engineering*, 313:450–482, 2017.

57. Tran Quoc Thai, Xiaoying Zhuang, Harold S Park, and Timon Rabczuk. A staggered explicit-implicit isogeometric formulation for large deformation flexoelectricity. *Engineering Analysis with Boundary Elements*, 122:1–12, 2021.

58. AK Tagantsev. Piezoelectricity and flexoelectricity in crystalline dielectrics. *Physical Review B*, 34(8):5883, 1986.

59. R Maranganti and P Sharma. Atomistic determination of flexoelectric properties of crystalline dielectrics. *Physical Review B*, 80(5):054109, 2009.

60. Massimiliano Stengel. Flexoelectricity from density-functional perturbation theory. *Physical Review B*, 88(17):174106, 2013.

61. Massimiliano Stengel. Surface control of flexoelectricity. *Physical Review B*, 90(20):201112, 2014.

62. Cyrus E Dreyer, Massimiliano Stengel, and David Vanderbilt. Current-density implementation for calculating flexoelectric coefficients. *Physical Review B*, 98(7):075153, 2018.

63. Pierre-Gilles deGennes and Jacques Prost. *The physics of liquid crystals*, volume 83. Oxford university press, 1993.

64. Robert B Meyer. Piezoelectric effects in liquid crystals. *Physical Review Letters*, 22(18):918, 1969.

65. Mrityunjay Kothari, Moon-Hyun Cha, and Kyung-Suk Kim. Critical curvature localization in graphene. i. quantum-flexoelectricity effect. *Proceedings of the Royal Society A: Mathematical, Physical and Engineering Sciences*, 474(2214):20180054, 2018.

66. Mrityunjay Kothari, Moon-Hyun Cha, Victor Lefevre, and Kyung-Suk Kim. Critical curvature localization in graphene. ii. non-local flexoelectricity–dielectricity coupling. *Proceedings of the Royal Society A*, 475(2221):20180671, 2019.

67. Alexander G Kvashnin, Pavel B Sorokin, and Boris I Yakobson. Flexoelectricity in carbon nanostructures: nanotubes, fullerenes, and nanocones. *The journal of physical chemistry letters*, 6(14):2740–2744, 2015.

68. Fatemeh Ahmadpoor and Pradeep Sharma. Flexoelectricity in two-dimensional crystalline and biological membranes. *Nanoscale*, 7(40):16555–16570, 2015.

69. Shashikant Kumar, David Codony, Irene Arias, and Phanish Suryanarayana. Flexoelectricity in atomic monolayers from first principles. *Nanoscale*, 2021.

70. Amartya S Banerjee and Phanish Suryanarayana. Cyclic density functional theory: A route to the first principles simulation of bending in nanostructures. *Journal of the Mechanics and Physics of Solids*, 96:605–631, 2016.

71. M Marvan and A Havránek. Static volume flexoelectric effect in a model of linear chains. *Solid state communications*, 101(7):493–496, 1997.

72. M Marvan and A Havránek. Flexoelectric effect in elastomers. In *Relationships of Polymeric Structure and Properties*, pages 33–36. Springer, 1998.

73. Sivapalan Baskaran, Xiangtong He, Yu Wang, and John Y Fu. Strain gradient induced electric polarization in α-phase polyvinylidene fluoride films under bending conditions. *Journal of Applied Physics*, 111(1):014109, 2012.

74. Baojin Chu and DR Salem. Flexoelectricity in several thermoplastic and thermosetting polymers. *Applied Physics Letters*, 101(10):103905, 2012.

75. L R G Treloar. *The physics of rubber elasticity*. Oxford University Press, 1975.

76. Paul J Flory. Network structure and the elastic properties of vulcanized rubber. *Chemical reviews*, 35(1):51–75, 1944.

77. Ellen M Arruda and Mary C Boyce. A three-dimensional constitutive model for the large stretch behavior of rubber elastic materials. *Journal of the Mechanics and Physics of Solids*, 41(2):389–412, 1993.

78. Mary C Boyce and Ellen M Arruda. Constitutive models of rubber elasticity: a review. *Rubber chemistry and technology*, 73(3):504–523, 2000.

79. Noy Cohen and Gal deBotton. Electromechanical interplay in deformable dielectric elastomer networks. *Physical review letters*, 116(20):208303, 2016.

80. Mikhail Itskov, Vu Ngoc Khiêm, and Sugeng Waluyo. Electroelasticity of dielectric elastomers based on molecular chain statistics. *Mathematics and Mechanics of Solids*, 2018.

81. Matthew Grasinger and Kaushik Dayal. Architected elastomer networks for optimal elec-

82. Matthew Grasinger and Kaushik Dayal. Architected elastomer networks for optimal electromechanical response. *Journal of the Mechanics and Physics of Solids*, page 104171, 2020. ISSN 0022-5096.

82. Matthew Grasinger and Kaushik Dayal. Statistical mechanical analysis of the electromechanical coupling in an electrically-responsive polymer chain. *Soft Matter*, 16:6265–6284, 2020.

83. Werner Kuhn and F Grün. Beziehungen zwischen elastischen konstanten und dehnungsdoppelbrechung hochelastischer stoffe. *Kolloid-Zeitschrift*, 101(3):248–271, 1942.

84. Michael J Lighthill. *An introduction to Fourier analysis and generalised functions*. Cambridge University Press, 1958.

85. Glenn Fredrickson et al. *The equilibrium theory of inhomogeneous polymers*, volume 134. Oxford University Press on Demand, 2006.

86. David R Lide. *CRC handbook of chemistry and physics*, volume 85. CRC press, 2004.

87. Ellad B Tadmor and Ronald E Miller. *Modeling materials: continuum, atomistic and multiscale techniques*. Cambridge University Press, 2011.

88. Hubert M James and Eugene Guth. Theory of the elastic properties of rubber. *The Journal of Chemical Physics*, 11(10):455–481, 1943.

89. Paul J Flory and John Rehner. Statistical mechanics of cross-linked polymer networks. ii. *The Journal of Chemical Physics*, 11:521–526, 1943.

90. PD Wu and Erik Van Der Giessen. On improved network models for rubber elasticity and their applications to orientation hardening in glassy polymers. *Journal of the Mechanics and Physics of Solids*, 41(3):427–456, 1993.

91. Noy Cohen, Kaushik Dayal, and Gal deBotton. Electroelasticity of polymer networks. *Journal of Mechanics Physics of Solids*, 92:105–126, 2016.

92. Matthew Grasinger. *Multiscale Modeling and Theoretical Design of Dielectric Elastomers*. PhD thesis, Carnegie Mellon University, 2019.

93. Matthew Grasinger, Carmel Majidi, and Kaushik Dayal. Nonlinear statistical mechanics drives intrinsic electrostriction and volumetric torque in polymer networks. *In preparation*.

94. Sivapalan Baskaran, Xiangtong He, Qin Chen, and John Y Fu. Experimental studies on the direct flexoelectric effect in α-phase polyvinylidene fluoride films. *Applied Physics Letters*, 98 (24):242901, 2011.

95. Eiichi Fukada and Saburo Takashita. Piezoelectric effect in polarized poly (vinylidene fluoride). *Japanese Journal of Applied Physics*, 8(7):960, 1969.

96. Kiran Kumar Sappati and Sharmistha Bhadra. Piezoelectric polymer and paper substrates: a review. *Sensors*, 18(11):3605, 2018.

97. MK Ashraf, Brent Millare, Alexander A Gerasimenko, Duoduo Bao, Rajeev R Pandey, Roger K Lake, and Valentine I Vullev. Theoretical design of bioinspired macromolecular electrets based on anthranilamide derivatives. *Biotechnology progress*, 25(4):915–922, 2009.

98. David J Griffiths. Introduction to electrodynamics, 2017.